Fischer–Tropsch synthesis: EXAFS study of Ru and Pt bimetallic Co based catalysts

C. Pirola [a,*], M. Scavini [a], F. Galli [a], S. Vitali [a], A. Comazzi [a], F. Manenti [b], P. Ghigna [c]

[a] Università degli Studi di Milano, Dipartimento di Chimica, Via Golgi 19, 20133 Milano, Italy
[b] Politecnico di Milano, Dipartimento di Chimica, Materiali e Ingegneria Chimica "Giulio Natta", Piazza Leonardo da Vinci 32, 20133 Milano, Italy
[c] Università degli Studi di Pavia, Dipartimento di Chimica, Viale Taramelli 16, 27100 Pavia, Italy

Article history:
Received 15 January 2014
Received in revised form 15 April 2014
Accepted 17 April 2014
Available online 2 May 2014

1. Introduction

Fischer–Tropsch Synthesis (FTS) is a well-known industrial process which starts from syngas (mixture of CO and H_2 obtained from CH_4, coal or, as a new tendency, biomass) for the production of light and heavy hydrocarbons [1]. Nowadays it is imperative to develop economical and energy-efficient processes for the sustainable production of fuels and chemicals alternative to the ones deriving from petroleum. FTS is a well-established industrial process through by means of which this aim can be achieved. FTS has been commercially used for many years and is still attracting much attention as a mean of producing transportation fuels due to the variety of raw materials that can be used as raw material

* Corresponding author. Tel.: +39 0250314293; fax: +39 0250314300.
E-mail address: carlo.pirola@unimi.it (C. Pirola).

for the syngas production [2,3]. FTS is now a crucial step in the Biomass-to-Liquid (BTL) process together with methanol synthesis [4–6]. The essential target of FTS is to produce paraffins and olefins with different molecular weights and to limit the maximum formation of methane and CO_2 [7]. FTS usually requires catalysts based on iron or cobalt [1]. Iron catalysts are often preferred over cobalt–based ones especially when converting syngas with molar H_2/CO ratio lower than 2 (the stoichiometric for FTS reaction) [8]. This is the typical condition when syngas is produced from biomass or coal [9]. Iron-based catalysts in fact are active towards the Water Gas Shift reaction (WGS: $CO + H_2O \leftrightarrow CO_2 + H_2$), able to produce hydrogen increasing in this way the H_2/CO ratio [10]. On the other hand when it is possible to feed in the FTS reactor a syngas mixture with a H_2/CO ratio close to 2 (syngas directly produced from natural gas or alternatively produced from coal or biomass and then enriched in H_2 by a proper shift reactor), cobalt catalysts are more largely used due to their both high selectivity to heavy hydrocarbons and low activity in WGS reaction limiting the CO_2 formation [11]. Moreover Co-based catalysts show longer life-time [12] and higher CO conversion compared with Fe based catalyst. Cobalt is traditionally supported in FTS catalyst. Promotion with platinum [13] and ruthenium [14] greatly increases the rate of cobalt reduction; the promotion seemed to reduce the activation energy of the formation of cobalt metallic phases [11,15,16].

Much experimental work has been devoted to investigate the microscopic structure of FTS catalysts, aiming to unveil the role of both Co and noble metals in this reaction. This is not a simple task due to the complex nature of the samples, which are composed by the support, Co both as in metallic and oxide form (~10 wt%) and the noble metal acting as a promoter (less than 2 wt%). An exhaustive structural investigation using powder diffraction is difficult and, in general, XRPD (X Ray Powder Diffraction) has been used to gain qualitative information. Conversely, EXAFS (Extended X-ray Absorption Fine Structure) has to be considered the suitable technique for this purpose due to its element selectivity. Also many groups have used EXAFS to characterize the microscopic nature of their FT catalysts on different supports. In particular, EXAFS experiments have been performed at the Co-K [13–22], at the Pt-L_{III} [17,20,23] and Ru-K [17–19] edges.

In the present work two sets of supported bimetallic and monometallic catalysts (BMCs and MMCs respectively) containing 10 wt% of Co and different percentages of Pt and Ru (0.1, 0.25, 0.5, and 2.0 wt%) were prepared in order to relate the catalytic performance of promoted Co catalysts to the nature and concentration of the noble metal promoters with particular attention to the structure, microstructure and distribution of Pt and Ru containing phases. TPR, SEM, TEM, XRPD and in particular EXAFS investigations were carried out on both promoted and unpromoted samples.

The catalytic performance was evaluated in a FTS laboratory-scale packed bed reactor, with particular attention to the effect of low quantity of noble metals (Ru and Pt) in BMCs. These catalysts are already well known in the literature and in the industrial applications, as pointed out. Nevertheless, the main aim of this paper is to provide a useful contribution to the state of the art of these catalytic systems, in particular in the understanding of their actual local structure by EXAFS analysis. The complementary characterization techniques together with the evaluation of FTS results of these materials are necessary to give a complete description of the system.

2. Material and methods

2.1. Catalysts preparation

The silica used as support was an Aldrich Product (diameter particles: 105–149 μm, BET surface: 500 $m^2\,g^{-1}$, pore volume: 0.75 $cm^3\,g^{-1}$); the salts used for the catalyst preparation were: Co (II) nitrate hexahydrate, Ru(III) and Pt(II) acethylacetonate, all Fluka products (purity >99.99%).

Both monometallic (MMCs) and bimetallic (BMCs) catalysts were prepared following the successive steps: support impregnation, air calcinations, reduction in hydrogen. All the percentages concerning the catalysts composition quoted in this paper are on weight basis. Co 10% on silica was prepared by impregnation using an aqueous solution of cobalt nitrate; before impregnation the support was heated overnight at 373 K. The impregnation was performed in a Rotavapor apparatus at 313 K, for 24 h. After the impregnation water was eliminated at 333 K in the same apparatus under moderate vacuum. The catalyst was then dried at 393 K and calcined at 773 K for 4 h in air using static conditions. The impregnation for Pt or Ru monometallic catalysts was made in the same way using acetone as solvent for the precursors. The bimetallic catalysts were prepared by a second impregnation with the Ru or Pt salts on Co 10%/SiO_2.

The symbol Co10 means a monometallic catalyst containing 10% of Co, i.e. [g Co/(g SiO_2 + g Co) × 100] = 10. For bimetallic catalysts the symbols Co*X*–Ru*Y* or Co*X*–Pt*Y* mean a catalyst prepared from 1 g of Co10 to which the cited precursors of Ru and Pt are added in order to give a ratio [g Ru/(1 g Co10 + g Ru)] × 100 = *Y* (where *Y* = 0.1 or other values as indicated in Table 1) and likewise for Pt.

The list of all the prepared samples is reported in Table 1.

2.2. Catalyst characterization

All the characterizations described in the following (SEM, TEM, XRPD, XPS, EXAFS) were performed on reduced samples. The prepared catalyst, after the calcination procedure was dried at 393 K, weighed and placed in a quartz reactor where it was fluxed with hydrogen (30 ml min^{-1}), while the temperature was raised to 633 K at 10 K min^{-1} and here maintained for 16 h, then it was fluxed with argon (30 ml min^{-1}) at 633 K for 2 h. Differently, TPR analysis were performed on the calcined sample. The reduction conditions were chosen in accord with a similar work by Dalil et al. [24].

The surface area of all catalysts was determined by conventional N_2 absorption at 77 K (BET method) using a Sorptometer 1042 instrument (Costech). Before the measurements, the catalyst samples were heated at 393 K for 12 h, and then pre-treated at 473 K in a nitrogen flux.

TPR/TPO Analysis: a cycle TPR1/TPO/TPR2 (Temperature Programmed Reduction/oxidation/reduction) was performed on the samples using a commercial apparatus (Thermoelectron) equipped

Table 1
Surface area and FTS results (*T* = 493 K) of all the prepared catalyst.

Sample	S.A. ($m^2\,g^{-1}$)	CO conversion (%)	Products selectivity (%)				C_2^+ yield (%)
			CO_2	CH_4	$\leqslant C_7$	$>C_7$	
Co10	369	21.4	1	6	8	84.7	19.8
Co10Pt0.1	365	66.3	2	7	7	85	52.8
Co10Pt0.25	358	66.6	3	6	8	85	60.8
Co10Pt0.5	359	68.7	3	7	8	82	62.8
Co10Pt2.0	356	63.9	6	9	8	74	54.6
Co10Ru0.1	349	54.6	2	6	9	73	50.2
Co10Ru0.25	346	66.3	2	7	8	81	60.3
Co10Ru0.5	353	71.2	2	6	6.7	85	65.3
Co10Ru2.0	336	42.7	6	9	11	62.7	35.4

$\leqslant C_7$: all the hydrocarbons in the range C_2–C_7.
$>C_7$: all the hydrocarbons greater than C_7.
Product "*i*" selectivity = (C moles in product *i*)/(C converted moles) × 100.
C_2^+ yield = CO conversion × ($\leqslant$C7 selectivity + $>C_7$ selectivity) × 10^{-2}.

with a TCD detector. The prepared catalysts, after the calcination procedure were dried at 393 K, then weighed and placed in a quartz reactor where they were fluxed with argon (30 ml min^{-1}), while the temperature was raised to 473 K at 10 K min^{-1} and then maintained at this temperature for one hour. The samples were cooled at room temperature in static air and the TPR1 procedure was performed feeding a flux (14 ml min^{-1}) of hydrogen in argon (5.01% V/V) and heating the sample from 323 to 1173 K (8 K min^{-1}); after reaching the last temperature the samples were cooled in the same gas to room temperature. Similarly, TPO was performed using a flux (14 ml min^{-1}) of oxygen in helium (5% V/V) from 323 to 1173 K just after TPR1. TPR2 procedure, after TPO, was the same as TPR1.

SEM, EDX, TEM: The surface morphology and phase distribution were investigated by using and Electron Scanning Microscope (SEM) Philips XL series – XL 30 ESEM-FEG. It is noteworthy to observe that this instrument can also work at atmospheric pressure, and that the combination ESEM-FED (Environmental Scanning Electron Microscopy – Field Emission Gun) increases the image contrast. TEM analyses were made on a Philips CM12 instrument equipped with a high-resolution camera.

XRPD: Room temperature XRPD patterns were collected between 5° and 80° (2θ range, $\Delta\theta$ = 0.017°) with an XPERT-PRO diffractometer (PANanalytical) equipped with a X' Celerator Position Sensitive detector for a total counting time of 1 h to collect each pattern. The diffractometer was operating with Cu Kα radiation (λ = 1.5418 Å) in Bragg Brentano (theta/theta) reflection geometry.

EXAFS: Fluorescence XAFS (X-ray Absorption Fine Structure) data were collected at the GILDA beamline [25] (European Synchrotron Radiation Facility, ESRF, Grenoble) at the Pt-L_{III} and Ru-K edges at room temperature. A Si (3 1 1) double crystal monochromator was used; to obtain a reasonable signal to noise ratio, the integration time was adjusted to obtain 10^6 counts in the fluorescence channel; in addition, in order to avoid distortions of the spectra, the count rate of each element was kept well below the saturation limit. The EXAFS data analysis was carried out taking advantage of the GNXAS [26,27] and EXCURV98 [28] programs. Full multiple scattering calculations making use of the exact curved wave theory were performed to fit the spectra. Backscattering and phase shifts were calculated by the program and take into account the Ramsauer–Towsend effect in at the Pt-L_{III} edge.

2.3. FTS laboratory-scale apparatus

FTS reaction tests have been carried out in a fixed bed tubular reactor, internal diameter = 6 mm, using 1 g of fresh catalyst mixed with 1 g of diluting material (α-Al_2O_3, Fluka). This diluting material is absolutely inert for FT both in term of activity and water adsorption [29]. Also, notwithstanding alumina is not a good thermal conductor, its presence allows a good control of the temperature inside the catalytic bed (the maximum increase of the temperature experimentally verified by an axial thermocouple was equal to 5 °C) [30].

All the catalysts were initially activated *in situ* in flowing H_2 (90.0 ml min^{-1} at 633 K, 0.8 MPa for 4 h). The catalysts were tested in a flow of syngas with H_2/CO (ratio of 2/1; flow = 46.8 Nml min^{-1}) using nitrogen as internal analytical standard (flow = 5.0 Nml min^{-1}) at 2.0 MPa and T = 493 K, for 90 h. Analysis of the gas-phase products (the fraction C_1–C_6 not condensed in the cold trap) were performed with an on-line microgaschromatograph (Agilent 3000A) equipped with two different columns: the first, a molsieves module, by which it is possible to separate CO, N_2 and CH_4 with a column temperature of 318 K, the second, a OV-1 module (filled with polydymethylsiloxilane), by which it is possible to separate CO_2 and all the hydrocarbons in the range C_2–C_6 with a column temperature of 373 K. In this instrument the gas sample is split into the two modules and then analyzed at the same time. Measurements were carried out every 60 min during the reaction.

Liquid products were collected, during the complete reaction cycle (90 h), in a trap (V = 400 ml), operating at 278 K and at the same pressure of the reactor (2.0 MPa), and then analyzed by a gas chromatograph (Fisons – 8000 series) equipped with a Porapack-Q columns (this being able to separate C_7–C_{30} hydrocarbon fraction). The column temperature was maintained at 333 K for 1 min and then heated up to 573 K at 8 K/min. The aqueous phase collected in the cold trap was analyzed by a TOC (Shimadzu 5000A) to identify the quantity of carbonaceous species dissolved in water. Using all the collected data, a molar balance resulted with a maximum error of ±5% moles, for each run.

3. Results and discussion

All the catalysts were characterized by TPR/TPO techniques in order to investigate their reduction/oxidation properties and verify the actual cooperation between cobalt and ruthenium or platinum in BMCs samples. Additionally a monometallic catalyst having 0.5% of Ru on silica (Ru0.5) and a mechanical mixture of cobalt 10% on silica and ruthenium 0.5% on silica (named Co10–Ru0.5/MM) were prepared as reference samples. TPR1/TPO/TPR2 plots of Co10 are reported in Fig. 1a, while in Fig. 1b TPR results are shown for the samples: Co10, Ru0.5, Co10–Ru0.5/MM. Similar plots are reported in Fig. 2 for the samples prepared by successive impregnation method: Fig. 2a for the Pt series (Co10, Co10–Pt0.1, Co10–Pt0.5, Co10–Pt2) and Fig. 2b for the Ru series (Co10, Co10–Ru0.1, Co10–Ru0.5, Co10–Ru2). Similar results are obtained for all the other mechanical mixtures and have not been reported for brevity. The numerical values of the peaks temperatures are given in Table 2.

An interesting difference between TPR1 and TPR2 plots in the monometallic Co10 can be observed in Fig. 1a; this indicates that after the TPO step a reconstruction of the surface is present. TPR1 plot (Fig. 1a) is very similar in comparison with that of Schanke et al. [31] (two peaks at 600 K and 670 K) while the peak 4 for TPR2 and 5 for TPO suggests that a new phase is present due to the possible formation of cobalt silicate, in accordance with the literature [32].

The sample Co10–Ru0.5MM (Fig. 1b) gives a TPR1 plot, which is almost the same as the sum of the two separate components, showing a total absence of metal–metal cooperation. On the contrary the supported Co–Pt and Co–Ru samples, obtained by successive impregnation, show a significant influence of the noble metal on the reduction temperature of cobalt oxides [33], and shown qualitatively in Fig. 2a and b respectively. Quantitative results are given in Table 2.

In particular, comparing Fig. 1b (Co10–Ru0.5MM, curve (b)) and 1b (Co10–Ru0.5, curve (c)) it is evident that a positive cooperative effect of Ru exists in the reduction of cobalt oxide(s) for the catalysts prepared by successive impregnation. In fact in Fig. 1b, curve (b) has the main peak 5, at T_5 = 664 K, while in Fig. 2b, curve (c) has the main peak 6, at T_6 = 629 K. Similar results were obtained comparing Co–Pt catalysts. All these results are qualitatively in agreement with literature [34–36]. The conclusion of TPR experiments is that the higher the noble metal concentration is in BMCs the lower the peaks temperatures are (Fig. 2: peaks 1–4 and 5–8, corresponding to the reductions $Co_3O_4 \rightarrow CoO$ and $CoO \rightarrow Co$, respectively). Therefore TPR results clearly demonstrate the presence of a strong spillover effect, which is well expected when a source of spilling species (e.g. a group of VIII metals) is coupled to an acceptor (e.g. an oxide) [37]. While for bulk Co_3O_4 the attribution of the peaks corresponding to the two previous reactions is possible [38], for

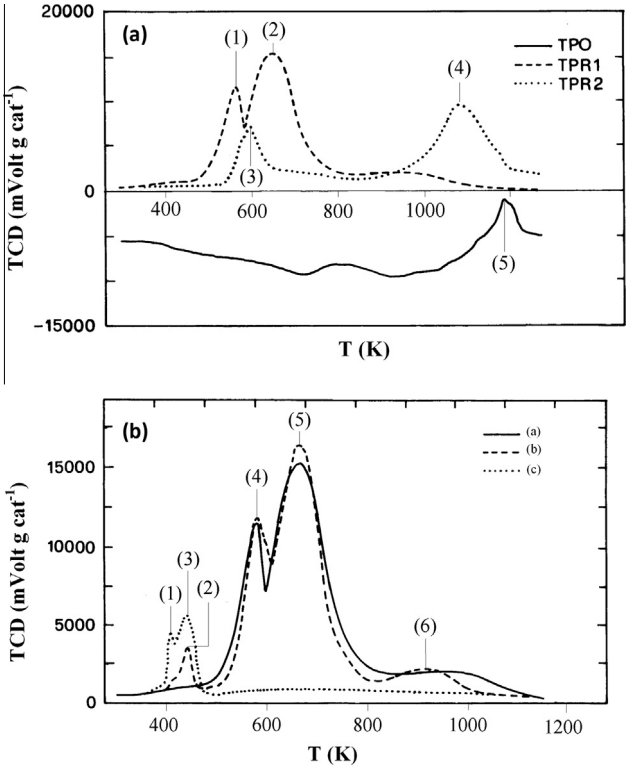

Fig. 1. a: TPR1/TPO/TPR2 plots of: Co10. Peak number/degree K: (1) 581; (2) 664; (3) 607; (4) 1099; (5) 1196; b: TPR of: (a) Co10, (b) Co10–Ru0.5MM (1:1) (MM, mechanical mixture), and (c) Ru0.5. Peak number/degree K: (1) 413; (2) 437; (3) 437; (4) 577; (5) 661; (6) 913.

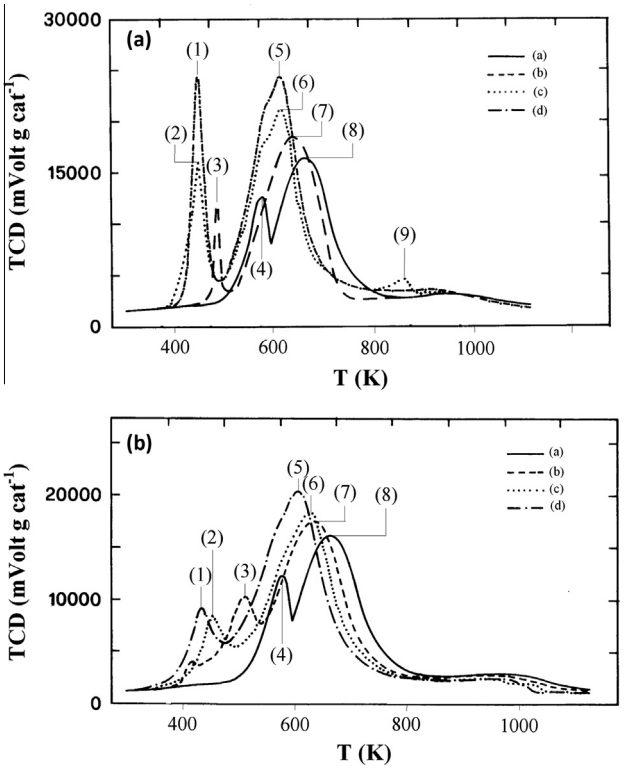

Fig. 2. a: TPR of Co10 and Co10–Pt*X* catalysts obtained by successive impregnation on Co10: (a) Co10, (b) Co10–Pt0.1, (c) Co10–Pt0.5, (d) Co10–Pt2. Peak number/degree K: (1) 447; (2) 449; (3) 486; (4) 518; (5) 618; (6) 619; (7) 643; (8) 670; (9) 929; b: TPR of Co10 and Co10–Ru*X* catalysts obtained by successive impregnation on Co10: (a) Co10, (b) Co10–Ru0.1, (c) Co10–Ru0.5, (d) Co10–Ru2. Peak number/degree K: (1) 436; (2) 455; (3) 517; (4) 580; (5) 609; (6) 623; (7) 639; (8) 670.

supported catalyst this is more difficult, being the step 2 $CoO \rightarrow 2Co + O_2$ dependent on both particle size and support properties connected with the retention of water produced by the reaction $Co_3O_4 + H_2 \rightarrow 3\ CoO + H_2O$.

Fig. 3 shows the SEM images of four reduced BMCs, [(a) Co10–Pt2, (b) Co10–Pt0.5, (c) Co10–Ru2 and (d) Co10–Ru0.5], while TEM images are shown in Fig. 4 for (a) Co10–Pt2 and (b) Co10–Ru2 samples as examples. SEM/EDX analyses of Co10–Pt*X* and Co10–Ru*X* (*X* = 0.5 and 2, Fig. 3a–d) show that the noble metal aggregates seem to grow mainly above the Co–Co_xO_y phase, in the reduced samples. This is undoubtedly a consequence of the preparation procedure, i.e. the cobalt precursor is deposited in the first step, then oxidized and finally the noble metal precursor is added. TEM analyses show larger Pt particles with respect to Ru ones.

In order to evaluate the crystalline structures of metallic phases XRPD analyses have been performed. Fig. 5 shows the diffraction patterns relative to Co10–Pt2 (A), Co10–Pt0.5 (B), Co10–Ru2 (C), Co10–Ru0.5 (D) and Co10 (E) samples. In addition to the contribution of amorphous SiO_2, only a few broad diffraction peaks are apparent in all the patterns. For what the Co10–Pt2 sample (pattern A in Fig. 5) concerns, aside the (1 1 1) reflection of cubic Co at ~44.5° and the (1 1 1) and (2 0 0) reflection of CoO, at 38.8° and 42.6° respectively, the (1 1 1) reflection of cubic Pt is apparent at ~40.0° This last peak disappears in the pattern relative to the Co10–Pt0.5 sample (see pattern B). The patterns relative to Co10–Ru2 (C), Co10–Ru0.5 (D) and Co10 (E) evidence the peaks relative to the Co and CoO phases. As a matter of fact the peaks of hexagonal metallic Ru could be hindered by those of CoO and Co ones since they fall at about the same angles [e.g. the Ru (1 0 1) reflection at ~44.0°]. Similarly the attribution of XRPD to Co_2SiO_4 phase is not possible because the position of the most intense diffraction peak of this phase is quite coincident with the CoO one.

Fig. 6 shows the EXAFS spectra for the samples Co10–Pt0.1 and Co10–Pt2 (a and c respectively), while the corresponding Fourier Transforms are shown in b and d, respectively. Similarly in Fig. 7 EXAFS spectra for the samples Co10–Ru0.1, Co10–Ru0.5, Co10–Ru2 are reported as a, c, e respectively, while in b, d and f the corresponding Fourier Transforms are shown, respectively. To better understand the local chemical environment of the supported noble metals in the BMCs, EXAFS analyses have been performed on Ru-K and Pt-L_{III} edges. With reference to Co10–Pt0.1 sample (Fig. 6a) the first peak in the Fourier Transforms (Fig. 6b) at about 2.5 Å *ca.* is attributed to Co atoms (nearest neighbors), while the second peak at about 3.0 Å *ca.* is attributed to Pt atoms (next nearest neighbors). Other peaks at higher distances are also found. The EXAFS evidence is therefore that for the Pt0.1 composition, Co and Pt form an intermetallic compound or a solid solution. In the Pt–Co phase diagram, a face centered cubic solid solution α and two intermetallic compounds (PtCo and Pt_3Co) can be obtained [39]. The best agreement between the observed and calculated EXAFS is achieved by using a structural model derived from the PtCo face centered tetragonal structure. The fit is shown in Fig. 6b as dotted lines, and the structural parameters obtained by the EXAFS analysis are shown in Table 3A. It can therefore be concluded that for the Co10–Pt0.1 composition, Pt forms the PtCo intermetallic compound.

On the contrary, the EXAFS spectrum of the Co10–Pt2 sample, which is show in Fig. 6c along with its Fourier transform (Fig. 6d), shows all the features of pure Pt and could be fitted using a structural model derived from the close packed cubic structure of Pt, as it is shown by the dotted lines in Fig. 6d. The structural parameters derived from the EXAFS analysis are displayed in Table 3B. The presence of metallic Pt in Co10–Pt2 samples is in perfect agreement with XRPD results (see Fig. 5).

With regard to the Co–Ru samples (Co10–Ru0.1, Co10–Ru0.5, Co10–Ru2, Figs. 7a, c and e respectively) all these spectra look very

Table 2
TPR peak temperatures. In parenthesis the peak numbers as referred to Figs. 2a and 4b.

Entry	wt% Pt	$Co_3O_4 \rightarrow CoO$ (K)	$CoO \rightarrow Co$ (K)	wt% Ru	$Co_3O_4 \rightarrow CoO$ (K)	$CoO \rightarrow Co$ (K)
1	0 (Co10)	575 (4)	660 (8)	0 (Co10)	575 (4)	662 (8)
2	0.1	485 (3)	635 (7)	0.1	508 (3)	636 (7)
3	0.5	449 (2)	615 (6)	0.5	451 (2)	629 (6)
4	2.0	449 (1)	611 (5)	2.0	433 (1)	605 (5)

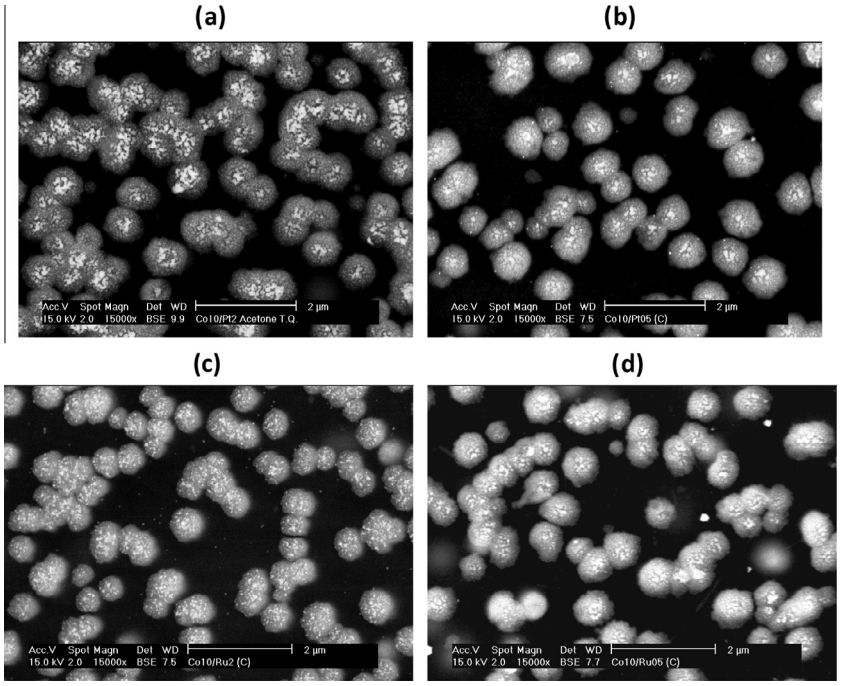

Fig. 3. SEM of reduced BMC samples (25·103X). White and grey particles are Pt and Ru on Co–Co_xO_y phase respectively as obtained by EDX; (a) Co10–Pt2, (b) Co10–Pt0.5, (c) Co10–Ru2, (d) Co10–Ru0.5.

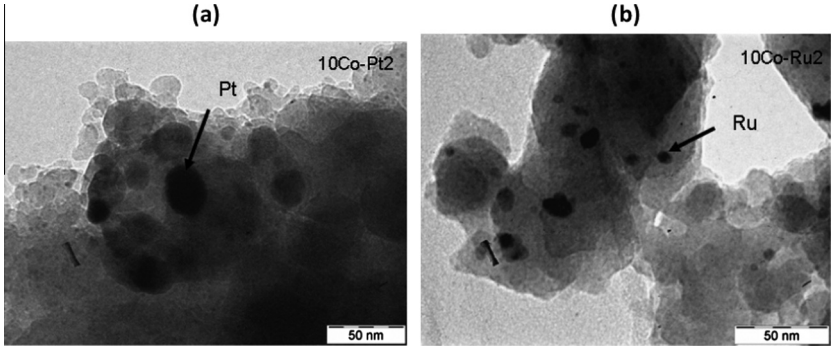

Fig. 4. TEM of reduced samples: (a) Co10–Pt2 and (b) Co10–Ru2.

similar and could be interpreted on the basis of the Ru hexagonal close packed structure. The structural parameters are displayed in Table 3C–E for the Co10–Ru0.1, Co10–Ru0.5 and Co10–Ru2 samples, respectively. It is clear that the Ru local chemical environment is impressively similar in the Co10–Ru0.1 and Co10–Ru2 samples, while the Co10–Ru0.5 sample is somewhat different. It is found in the literature [40] that Co and Ru form a continuous series of solid solutions having hexagonal close packed structure, their lattice constants being situated on a straight line connecting the constants of the components. As the distance of the first shell in the hcp structure is equal to the lattice constant, we can use the values displayed in Table 3C–E to obtain a composition of the solid solution in the bimetallic Ru/Co catalysts. Using the value 2.5071 Å and 2.7059 Å, for Co and Ru, respectively [40,41], it is found that the Co10–Ru0.1 and Co10–Ru2 samples contain Ru–Co alloys having ca. 23% (atomic percentage) of Co, while in the Co10–Ru0.5 samples the alloy is much richer in Ru, and contain only ca. 10% (atomic percentage) of Co.

Although this can be regarded as indirect results, and cannot be directly confirmed by fitting the spectra using different models, due to the intrinsic limitations of the EXAFS technique, good evidence in support of this conclusion can be obtained by looking at the intensity of the main peak in the Fourier Transforms in Fig. 7b, d, and f. It is fairly evident that for the Co10–Ru0.1 and

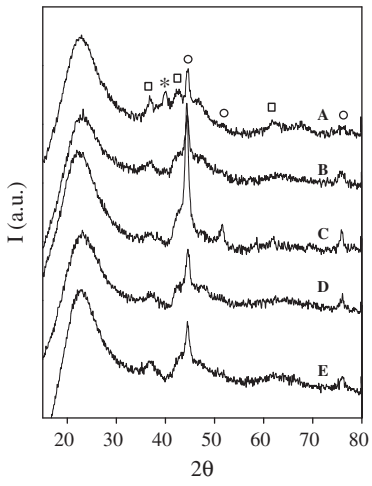

Fig. 5. XRPD power diffraction patterns of samples reduced for 3 h at 623 K in hydrogen atmosphere: A: Co10–Pt2; B: Co10–Pt0.5, C: Co10–Ru2; D: Co10–Ru0.5; E: Co10. The symbols indicate the diffraction peaks relative to: hexagonal Co (circles); CoO (square) and Pt (asterisks).

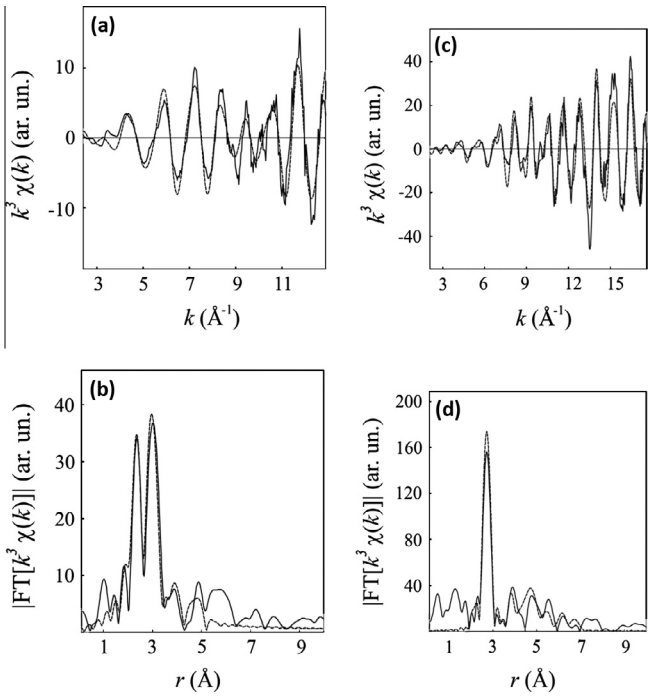

Fig. 6. a and c: Pt-L_{III} edge EXAFS signal for the Co10–Pt0.1 and Co10–Pt2 respectively samples. b and d: The corresponding Fourier transform. Full lines: experimental; dotted lines fit obtained as indicated in the text. Multiple scattering contributions are clearly apparent at high r ($\geqslant$5 Å).

Co10–Ru2 samples the intensity are quite the same, while for the Co10–Ru0.5 sample a much higher intensity is found. The intensity of the peaks in the EXAFS Fourier Transform reflects both the number of neighbors and the magnitude of their backscattering functions. Variations in the number of neighbors originated by changes in the size of the particles can be excluded on the basis of SEM and TEM inspections of samples. Thus, the only possible explanation for the above mentioned increase in amplitude is the presence of a lesser amount of Co in the Co10–Ru0.5 sample, provided that the backscattering function of Co is (on average) lower than that of Ru.

Fig. 8 summarizes the hypotheses regarding the structure of Co–Pt and Co–Ru ensembles as derived from the above reported discussion of EXAFS measurements. Obviously Fig. 8 drawings of the ensembles do not represent the overall composition of the cited samples because EXAFS probes the radial distribution function of Ru and Pt atoms of the ensembles and therefore this technique gives only the local chemical environment around the noble metals, up to a distance of few Å.

Basically the structure of Co–Pt and Co–Ru ensembles are different. Clusters in which Co and Pt atoms coexist forming PtCo compound (in Co10–Pt0.1) or only Pt atoms form cubic Pt phase (in Co10–Pt2) are present (see Fig. 8). In the latter case a long-range migration of hydrogen through a spill-over process may happen as indicated in bimetallic catalysts of Co with Ir, Ru, Rh, Re, Pt or Os supported on silica [42]. For what concerns BMCs, Ru based, solid solutions Co_xRu_y are present (see previous discussion and Fig. 8). Moreover a Ru-richer solid solutions is present in Co10–Ru0.5 sample having an atomic percentage of about 90% of Ru and 10% Co.

Guczi et al. [43] have studied the behavior for hydrogen chemisorption of cobalt–platinum bimetallic catalysts on alumina using both calcined and reduced samples. In this study the catalysts have different Pt/Co atomic ratio (total metal loading 10%): 15/85 (i.e. 0.176/1); 33/67 (i.e. 0.493/1); 50/50 (i.e. 1/1); 80/20 (i.e. 4/1). For the two samples with Co > Pt (the samples of the present study were however Co $\gg$ Pt), in order to justify the platinum-assisted reduction of Co_3O_4 species in the Co–Pt oxidized samples, an intimate contact between metallic platinum and cobalt particles was assumed, being the highly dispersed platinum partly covered by metallic cobalt. Moreover the presence of bimetallic particles detected by EXAFS on $Pt_{0.6}Co_{0.04}$ sample was reported [44]. Undoubtedly our TPR results (Fig. 2a) agree with those of Guczi's paper regarding the formation of intimate contact between Co and Pt in the very diluted samples with respect to Pt (Co $\gg$ Pt as in our samples: i.e. Co10–Pt0.05 or Co10–Pt0.1, corresponding to an atomic ratio Co 666/Pt 1 and Co 333/Pt 1 respectively).

As to the catalytic performance of the above materials, FTS results are presented in Table 1 in term of CO conversion and selectivity toward CO_2, CH_4, light hydrocarbons ($<C_7$: having less than 7 carbon atoms) and heavy hydrocarbons ($>C_7$: having more than 7 carbon atoms). Furthermore, the combination of the results of both the CO conversion and products selectivity is taken into account calculating the total yield to C^{2+} hydrocarbons, i.e. not considering methane and carbon dioxide since they are usually regarded as undesired products in the FT process (see notes in Table 1). FTS data were collected when the reaction reached the stationary state (i.e. constant values of CO conversion and products selectivity), about 24 h after the run start. After this initial step, both conversion and selectivity remained steady, suggesting good catalysts stability for the whole duration of each single run (90 h).

In Fig. 9 CO conversion and selectivity towards desired products are reported as key parameters to evaluate the performance of the different samples. By observing the numerical values, it is possible to conclude that the effect of the Ru and Pt addition is to increase the catalytic activity. In fact both CO conversion and hydrocarbon yields are approximately tripled. The effect of Pt and Ru seems to be quite the same. Nevertheless, this positive effect seems to be independent from the quantity of noble metal present in BMCs catalysts, being also the lower quantity added (0.1%) enough to get the full advantage of using a bimetallic catalyst (both BMCs samples with 2% of Ru and Pt give CO conversion and C^{2+} yield values lower than the corresponding sample with 0.1% of noble metal). The selectivity of cobalt based catalysts is highly dependent from the operative conditions (temperature, space velocity, catalyst composition, H_2/CO ratio in the feed), as highlined by Dalil et al. [24] for what concerns the yield towards heavy products.

It is not easy to correlate these FTS results with some particular BMCs structural property, being these systems very complex in

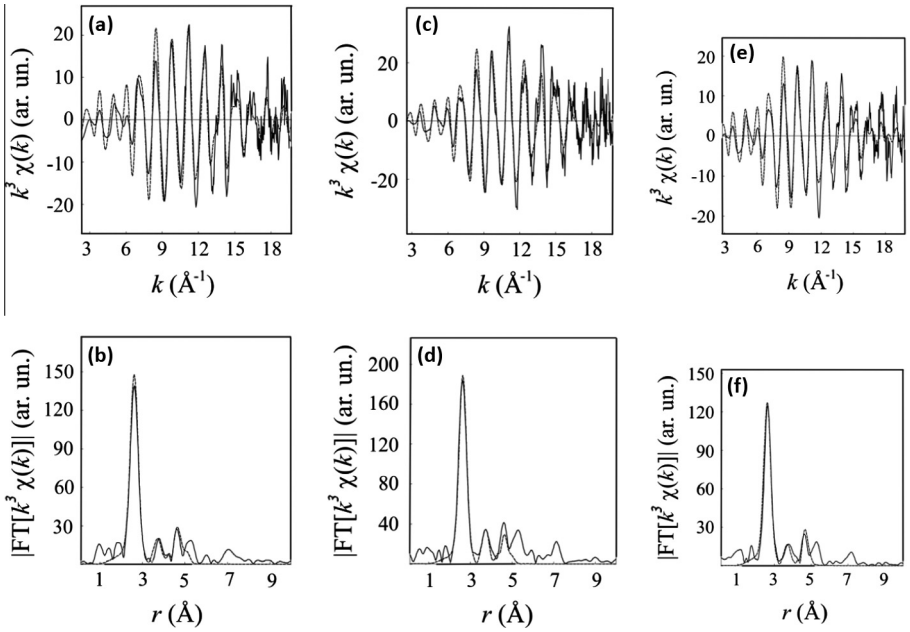

Fig. 7. a, c, and e: Ru-K edge EXAFS signal for Co10–Ru0.1, Co10–Ru0.5, Co10–Ru2 samples respectively b, d, f: the corresponding Fourier transform. Full lines: experimental; dotted lines fit obtained as indicated in the text. Multiple scattering contributions are clearly apparent at high r (>5 Å).

Table 3
EXAFS fitting parameters for spectra of Figs. 6 and 7.

Shell	Atom	r (Å)	σ^2 (Å^2)	N
(A) Fig. 6a (Co10–Pt0.1) r: distances; σ^2: distance variances N: coordination numbers				
1	Co	2.55 (1)	0.029 (1)	8
2	Pt	2.745 (6)	0.0057 (6)	4
3	Pt	3.60 (3)	0.012 (6)	2
4	Pt	3.86 (6)	0.03 (1)	4
(B) Same as Table 2A but for the spectrum of Fig. 6c (Co10–Pt2)				
1	Pt	2.766 (3)	0.0070 (2)	12
2	Pt	3.90 (1)	0.009 (1)	6
3	Pt	4.82 (2)	0.014 (2)	24
4	Pt	4.47 (3)	0.012 (3)	12
5	Pt	6.19 (3)	0.015 (5)	24
6	Pt	6.79 (3)	0.007 (4)	8
(C) Same as Table 2A but for the spectrum of Fig. 7a (Co10–Ru0.1)				
1	Ru	2.661 (4)	0.0122 (4)	12
2	Ru	3.75 (1)	0.014 (3)	6
3	Ru	4.449 (9)	0.003 (1)	2
4	Ru	4.643 (3)	0.015 (2)	18
(D) Same as Table 2A but for the spectrum of Fig. 7c (Co10–Ru0.5)				
1	Ru	2.680 (4)	0.0100 (4)	12
2	Ru	3.77 (1)	0.0010 (2)	6
3	Ru	4.47 (1)	0.002 (1)	2
4	Ru	4.68 (1)	0.015 (2)	18
(E) Same as Table 2A but for the spectrum of Fig. 7e (Co10–Ru2)				
1	Ru	2.661 (4)	0.0135 (4)	12
2	Ru	3.75 (2)	0.016 (3)	6
3	Ru	4.46 (1)	0.004 (2)	2
4	Ru	4.65 (1)	0.015 (1)	18

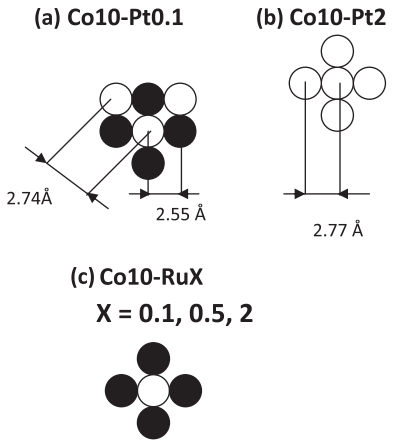

Fig. 8. Hypotheses of the Co–Pt and Co–Ru ensembles structure in the bimetallic samples as deduced from EXAFS analyses. White circles represent sites occupied by Pt or Ru; black circles represent Co atoms. Circles with white and black colors inside represent sites which can be occupied by either Ru and Co atoms (solid solutions in which the different percentages of Ru is discussed in the text (see paragraph 4.5). (a) Pt–Co intermetallic compound; (b) metallic platinum ensemble; (c and d) Co–Ru: alloys.

terms of different surface area, morphology, oxidation state, dispersion of the active particles on the support and so on. Nevertheless, with particular reference to the influence of the noble metal amount in the FTS catalytic performance, shown in Fig. 9 and above discussed, it is worth noting that the structural evolution of noble metal containing phases is different for Ru and Pt. In Ru based BMCs, the ruthenium environment does not change much at varying Ru amount: $Ru_{1-y}Co_y$ solid solutions with hexagonal close packed structure form were identified with y in the 0.1–0.23 range for all the concentration of noble metal. On the contrary, in the Pt based BMCs, the structure of Pt containing phase is strongly dependent on the amount of Pt: for low amount of Pt (0.1%) Co and Pt form the intermetallic compound PtCo with a face centered tetragonal structure while the EXAFS spectrum of the sample with higher loading of Pt (2%), could be fitted using a structural model derived from the close packed cubic structure of Pt. The main FTS result, i.e. very low amount of Pt and Ru (0.1 wt%) are required to obtain the fully performance advantage in bimetallic samples, should indicate that the local structures, determined by EXAFS in the BMCs with lower noble metal loading ($Ru_{1-y}Co_y$ solid solutions with hexagonal close packed structure for Ru BMCs and intermetallic compound PtCo with a face centered tetragonal structure for Pt BMCs) are the most suitable for the interaction of cobalt/ruthenium and cobalt/platinum interactions in FTS mechanism. A further increase

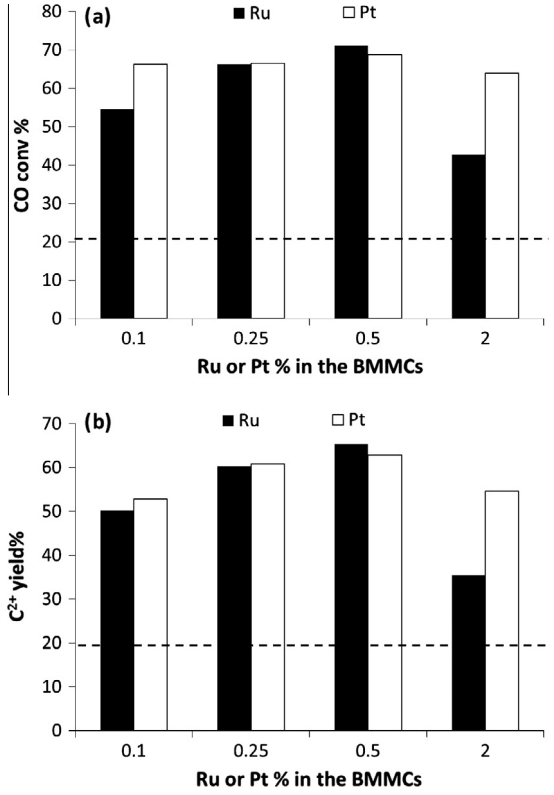

Fig. 9. FTS results. CO conversion 5 (a) and C^{2+} yield% (b) vs. Ru or Pt wt percentage in BMCs catalysts. The dotted line represents the value obtained using MMC catalyst (Co10).

in noble metal content is not convenient in term of FTS products, resulting in similar (Pt) or worse (Ru) results.

4. Conclusion

Co/Ru and Co/Pt bimetallic catalysts (BMCs) supported on silica were prepared, characterized and tested in Fischer Tropsch Synthesis (FTS) reaction. TPR/TPO/TPR and EXAFS analysis were applied to understand the actual cooperation of the different metals. FTS results showed that both CO conversion and the total yield towards desired products could be tripled thanks to the action of the noble metal, present in low amount on the catalysts composition. EXAFS analysis demonstrated different interactions of the two noble metals with cobalt in BMCs. As to Co/Ru catalysts, $Ru_{1-y}Co_y$ solid solutions with hexagonal close packed structure form were identified with y in the 0.1–0.23 range for all the concentration of noble metal. Differently in the Co/Pt BMCs, the structure of Pt containing phase is strongly dependent on Pt amount: for low Pt amount (0.1%) Co and Pt form the intermetallic compound PtCo with a face centered tetragonal structure while the EXAFS spectrum of the sample with higher loading of Pt (2%) could be fitted using the a structural model derived from the close packed cubic structure of Pt. The local structures identified with low loading of noble metal in BMCs are the most suitable for the interaction of cobalt/ruthenium and cobalt/platinum interactions in FTS mechanism.

Acknowledgements

The Authors are very grateful to Prof. Vittorio Ragaini for the helpful discussions.

References

[1] Bartholomew CH. Recent technological developments in Fischer–Tropsch catalysis. Catal. Lett. 1990;7(1–4):303–15.
[2] Ranzi E, Corbetta M, Manenti F, Pierucci S. Kinetic Modeling of the Thermal Degradation and Combustion of Biomass. Chem Eng Sci 2013. http://dx.doi.org/10.1016/j.ces.2013.08.014.
[3] Fu T, Jiang Y, Lv J, Li Z. Effect of carbon support on Fischer–Tropsch synthesis activity and product distribution over Co-based catalysts. Fuel Process Technol 2013;110:141–9.
[4] Manenti F, Garcon-Leon A, Bozzano G. Energy-process integration of the gas-cooled/water-cooled fixed-bed reactor network for methanol synthesis. Chem Eng Trans 2013;35:1243–8.
[5] Manenti F, Cieri S, Restelli M, Bozzano G. Dynamic modelling of the methanol synthesis fixed-bed reactor. Comput Chem Eng 2013;48:325.
[6] Manenti F, Cieri S, Restelli M. Considerations on the steady-state modeling of methanol synthesis fixed-bed reactor. Chem Eng Sci 2011;66:152.
[7] Zhang Q, Kang J, Wang Y. Development of novel catalysts for Fischer–Tropsch synthesis: tuning the product selectivity. Chem Cat Chem 2010;2:1030.
[8] Rao VUS, Stiegel GJ, Cinquegrane GJ, Srivastava RD. Iron-based catalysts for slurry-phase Fischer–Tropsch process: technology review. Fuel Process Technol 1992;30(1):83–107.
[9] Gardezi SA, Joseph B, Prado F, Barbosa A. Thermochemical biomass to liquid (BTL) process: bench scale experimental results and projected process economics of a commercial scale process. Biomass Bioenergy 2013;59:168–86.
[10] Abello S, Montane D. Exploring iron-based multifunctional catalysts for Fischer–Tropsch synthesis: a review. Chem Sus Chem 2011;4(11):1538–56.
[11] Diehl F, Khodakov AY. Promotion of cobalt Fischer–Tropsch catalysts with noble metal: a review. Oil Gas Sci Technol 2009;64(1):11–24.
[12] Hirsa M, Torres G, Krijn P. Catalysts for production of lower olefins from synthesis gas: a review. ACS catal 2013;3:2130–49.
[13] Chu W, Chernavskii PA, Gengembre L, Pankina GA, Fongarland P, Khodakov AY. Cobalt species in promoted cobalt alumina-supported Fischer–Tropsch catalysts. J Catal 2007;252:215.
[14] Girardon JS, Quinet E, Griboval-Constant A, Chernavskii PA, Gengembre L, Khodakov AY. Cobalt dispersion, reducibility, and surface sites in promoted silica-supported Fischer–Tropsch catalysts. J Catal 2007;248:143.
[15] Cronauer DC, Elam JW, Kropf AJ, Marshall CL, Gao P, Hopps S, et al. Fischer–Tropsch synthesis: preconditioning effects upon Co-containing promoted and unpromoted catalysts. Catal Lett 2012;142:698.
[16] Diehl F, Khodakov AY. Promotion of cobalt Fischer–Tropsch catalysts with noble metals: a review. Oil Gas Sci Technol 2009;64:11.
[17] Jacobs G, Sarkar A, Ji Y, Luo M, Dozier A, Davis BH. Fischer–Tropsch synthesis: assessment of the ripening of cobalt clusters and mixing between Co and Ru promoter via oxidation-reduction cycles over lower Co-loaded Ru–Co/Al_2O_3 catalysts. Ind Eng Chem Res 2008;47:672.
[18] Ma W, Jacobs G, Ji Y, Bhatelia T, Bukur DB, Khalid S, et al. Fischer–Tropsch synthesis: influence of CO conversion on selectivities, H_2/CO usage ratios, and catalyst stability for a Ru promoted Co/Al_2O_3 catalyst using a slurry phase reactor. Topics Catal 2011;54:757.
[19] Rochet A, Moizan V, Pichon C, Diehl F, Berliet A, Briois V. In situ and operando structural characterization of a Fischer–Tropsch supported cobalt catalyst. Catal Today 2011;171:186.
[20] Guczi L, Bazin D, Kovacs I, Borko L, Scay Z, Lynch J, et al. Structure of Pt–Co/Al_2O_3 and Pt–Co/NaY bimetallic catalysts: characterization by in situ EXAFS, TPR, XPS and by activity in Co (carbon monoxide) hydrogenation. Topics Catal 2002;20:129–39.
[21] Bazin D, Kovacs I, Lynch J, Guczi L. Ru–Co/NaY bimetallic catalysts: in situ EXAFS study at Co K- and Ru K-absorption edges. Appl Catal A: Gen 2003;242:179–86.
[22] Jacobs G, Ma W, Gao P, Todic B, Bhatelia T, Bukur DB, et al. Fischer–Tropsch synthesis: influence of CO conversion on selectivities, H_2/CO usage ratios, and catalyst stability for a Ru promoted Co/Al_2O_3 catalyst using a slurry phase reactor. Topics Catal 2012;55:811.
[23] Lu S, Lonergan WW, Zhu Y, Xie Y, Chen JG. Support effect on the low-temperature hydrogenation of benzene over PtCo bimetallic and the corresponding monometallic catalysts. Appl Catal B: Environ 2009;91:610.
[24] Dalil M, Sohrabi M, Royiaii SJ. Application of nano-sized cobalt on ZSM-5 zeolite as an active catalyst in Fischer–Tropsch synthesis. J Ind Eng Chem 2012;18:690–6.
[25] D'acapito F, Colonna S, Pascarelli S, Antonioli G, Balerna A, Bazzini A, Boscherini F, Campolungo F, Chini G, Dalba G, Davoli GI, Fornasini P, Graziola R, Licheri G, Meneghini C, Rocca F, Sangiornio L, Sciarra V, Tullio V, Mobilio S. GILDA (Italian beamline) on BM8. (1998) ESRF Newsletter 1998; 30: 42.
[26] Filipponi A, Di Cicco A, Natoli CR. X-ray absorption spectroscopy and n-body distribution functions in condensed matter (I): theory of the GNXAS data-analysis method. Phys Rev B 1995;52:15122.
[27] Filipponi A, Di Cicco A. X-ray absorption spectroscopy and n-body distribution functions in condensed matter (II): applications of the GNXAS data-analysis method. Phys Rev 1995;B 52:15135.
[28] Binsted N, Gurman SJ, Campbell TC, Stephenson PC. EXCURV98 program (Daresbury: SERC Daresbury Laboratory); 1998.

[29] Bianchi CL, Ragaini V, Pirola C. Choosing the best diluent for a fixed catalytic bed: the case of CO hydrogenation. Catal Commun 2006;7:669.
[30] Di Fronzo A, Pirola C, Comazzi A, Galli F, Bianchi CL, Di Michele A, et al. Co-based hydrotalcites as new catalysts for the Fischer–Tropsch synthesis process. Fuel 2014;119:62–9.
[31] Schanke D, Vada S, Blekkan E, Hilmen AM, Hoff A, Holmen A. Study of Pt-promoted Cobalt CO hydrogenation catalyst. J Catal 1995;156:85.
[32] Ernst B, Bensaddik A, Hilaire L, Chaumette P, Kiennemann A. Study on a cobalt silica catalyst during reduction and Fischer–Tropsch reaction: in situ EXAFS compared to XPS and XRD. Catal Today 1998;39:329.
[33] Khodakov AY, Chu W, Fongarland PF. Advances in the development of novel cobalt Fischer–Tropsch catalysts for synthesis of long chain hydrocarbons and clean fuels. Chem Rev 2007;107:1692.
[34] Jacobs G, Das TK, Zhang Y, Li J, Racoillet G, Davis BH. Fischer–Tropsch synthesis: support, loading and promoter effects on the reducibility of Co-catalyst. Appl Catal A: Gen 2002;233:263.
[35] Tsubaki N, Sun S, Fujmoto K. Different function of novel metal added to cobalt catalyst for the Fischer–Tropsch synthesis. J Catal 2001;199:236.
[36] Iglesia E, Soled SL, Fiato RA, Via GH. Bimetallic synergy in cobalt–ruthenium Fischer–Tropsch synthesis catalysts. J Catal 1993;143:345–68.
[37] Curtis W, Conne J. Hydrogen effects in catalysis. New York: Marcel Dekker; 1988 [Chapter 12].
[38] Anderson JR, Pratt KC. Introduction to characterization and testing of catalysts. North Ryde: Academic Press; 1985.
[39] Hansen M, Anderko K. Constitution of binary alloys. 2nd ed. New York: Mcgraw-Hill; 1958.
[40] Vincent F, Figlarz M, Hebd CR. Quelques précisions sur les paramètres cristallins et l'intensité des raies Debye–Scherrer du cobalt cubique et du cobalt hexagonal. Acad Sci 1967;264:1270.
[41] Finkel A, Palatnik MI, Kovtun GP. X-ray diffraction study of the thermal expansion of Ru, Os and Re at 77–300 K. Phys Met Metall 1971:32–121.
[42] Matzusaki T, Takeuchi K, Hanaoka T, Arakawa H, Sugi Y. Hydrogenation of carbon monoxide over highly dispersed cobalt catalysts derived from cobalt(II) acetate. Catal Today 1996;28:251.
[43] Guczi L, Hoffer T, Zsoldos Z, Zyade S, Maire G, Garin F. Structure and catalytic activity of supported Pt–Co bimetallic catalysts. Part 2. Chemisorption and catalytic reactions. J Phys Chem 1991;95:802.
[44] Zyade S, Garin F, Maire G. Isomerization and hydrogenolysis mechanisms of C6 alkanes on bimetallic platinum–cobalt systems. New J Chem 1987;11(5):429–35.